





## ORIGINAL ARTICLE

OPEN

# RIPK3 dampens mitochondrial bioenergetics and lipid droplet dynamics in metabolic liver disease

Marta B. Afonso<sup>1</sup>  | Tawhidul Islam<sup>1</sup> | Julie Magusto<sup>2,3</sup> | Ricardo Amorim<sup>4</sup> |  
 Véronique Lenoir<sup>5</sup> | Rui F. Simões<sup>4</sup> | José Teixeira<sup>4</sup> | Liana C. Silva<sup>1</sup> |  
 Dominique Wendum<sup>3,6</sup> | Isabelle Jéru<sup>2,3,7</sup> | Corinne Vigouroux<sup>2,3,8</sup> |  
 Rui E. Castro<sup>1</sup> | Paulo J. Oliveira<sup>4</sup>  | Carina Prip-Buus<sup>5</sup> | Vlad Ratziu<sup>2,9,10</sup>  |  
 Jérémie Gautheron<sup>2,3</sup> | Cecília M. P. Rodrigues<sup>1</sup> 

<sup>1</sup>Research Institute for Medicines (iMed.Ulisboa), Faculty of Pharmacy, Universidade de Lisboa, Lisbon, Portugal

<sup>2</sup>Institute of Cardiometabolism and Nutrition, Paris, France

<sup>3</sup>Sorbonne Université, Inserm, Centre de Recherche Saint-Antoine, Paris, France

<sup>4</sup>CNC - Center for Neuroscience and Cell Biology, University of Coimbra, Coimbra, Portugal

<sup>5</sup>Université de Paris, Institut Cochin, INSERM, CNRS, Paris, France

<sup>6</sup>Service d'Anatomo-Pathologie, Service d'Hépatologie, Centre de Référence Maladie Rare Maladies Inflammatoires des Voies Biliaires-Hépatites Auto-immunes, Paris, France

<sup>7</sup>Laboratoire commun de Biologie et Génétique Moléculaires, Hôpital Saint-Antoine, Paris, France

<sup>8</sup>Centre National de Référence des Pathologies Rares de l'Insulino-Sécrétion et de l'Insulino-Sensibilité, Service de Diabétologie et Endocrinologie de la Reproduction, Hôpital Saint-Antoine, Paris, France

<sup>9</sup>Department of Hepatology, Assistance Publique-Hôpitaux de Paris, Pitié-Salpêtrière Hospital, Paris, France

<sup>10</sup>Sorbonne Université, Inserm, Centre de Recherche des Cordeliers, and ICAN Institute of Cardiometabolism and Nutrition, Paris, France

## Correspondence

Cecília M. P. Rodrigues, iMed.Ulisboa, Faculty of Pharmacy, Universidade de Lisboa, Av. Prof. Gama Pinto, 1649-003 Lisbon, Portugal.  
 Email: [cmprodriues@ff.ulisboa.pt](mailto:cmprodriues@ff.ulisboa.pt)

## Funding information

Agence Nationale de la Recherche, Grant/Award Number: ANR-21-CE18-0002-01; Fondation pour la Recherche Médicale, Grant/Award Number: ARF20170938613 & EQU202003010517; Fundação para a Ciência e a Tecnologia, Grant/Award Number: PTDC/MED-FAR/29097/2017 -LISBOA-01-0145-FEDER-029 and SAICTPAC/0019/2015-LISBOA-01-0145-FEDER-016405; H2020 Marie Skłodowska-Curie Actions, Grant/Award

## Abstract

**Background and Aims:** Receptor-interacting protein kinase 3 (RIPK3) mediates NAFLD progression, but its metabolic function is unclear. Here, we aimed to investigate the role of RIPK3 in modulating mitochondria function, coupled with lipid droplet (LD) architecture in NAFLD.

**Approach and Results:** Functional studies evaluating mitochondria and LD biology were performed in wild-type (WT) and *Ripk3*<sup>-/-</sup> mice fed a choline-deficient, amino acid-defined (CDAA) diet for 32 and 66 weeks and in CRISPR-Cas9 *Ripk3*-null fat-loaded immortalized hepatocytes. The association between hepatic perilipin (PLIN) 1 and 5, RIPK3, and disease severity

**Abbreviations:** Acc, acetyl-CoA carboxylase; CDAA, choline-deficient, amino acid-defined; CSAA, choline-sufficient L-amino acid-defined; DEG, differentially expressed gene; FPLD, familial partial lipodystrophy; LD, lipid droplet; MFN2, mitofusin 2; MLKL, mixed lineage kinase domain-like protein; MRC, mitochondria respiratory chain; OCR, oxygen consumption rate; OXPHOS, oxidative phosphorylation; PA, palmitate; PGC1 $\alpha$ , proliferator-activated receptor gamma coactivator 1 alpha; PLIN, perilipin; PPAR $\gamma$ , peroxisome proliferator-activated receptor  $\gamma$ ; RIPK3, receptor-interacting protein kinase 3; ROS, reactive oxygen species; RT-PCR, reverse transcriptase-polymerase chain reaction; TMRM, tetramethylrhodamine methyl ester perchlorate; WT, wild-type.

Marta B. Afonso, Tawhidul Islam, and Julie Magusto contributed equally to this work.

Supplemental Digital Content is available for this article. Direct URL citations appear in the printed text and are provided in the HTML and PDF versions of this article on the journal's website, [www.hepjournal.com](http://www.hepjournal.com).

This is an open access article distributed under the terms of the Creative Commons Attribution-Non Commercial-No Derivatives License 4.0 (CCBY-NC-ND), where it is permissible to download and share the work provided it is properly cited. The work cannot be changed in any way or used commercially without permission from the journal.

Copyright © 2023 The Author(s). Published by Wolters Kluwer Health, Inc.

Number: 722619; Mairie de Paris, Grant/Award Number: Emergences -R18139DD; La Caixa Foundation, Grant/Award Number: LCF/PR/HR21/52410028.

was also addressed in a cohort of patients with NAFLD and in *PLIN1*-associated familial partial lipodystrophy. *Ripk3* deficiency rescued impairment in mitochondrial biogenesis, bioenergetics, and function in CDAA diet-fed mice and fat-loaded hepatocytes. *Ripk3* deficiency was accompanied by a strong upregulation of antioxidant systems, leading to diminished oxidative stress upon fat loading both in vivo and in vitro. Strikingly, *Ripk3*<sup>-/-</sup> hepatocytes displayed smaller size LD in higher numbers than WT cells after incubation with free fatty acids. *Ripk3* deficiency upregulated adipocyte and hepatic levels of LD-associated proteins PLIN1 and PLIN5. PLIN1 upregulation controlled LD structure and diminished mitochondrial stress upon free fatty acid overload in *Ripk3*<sup>-/-</sup> hepatocytes and was associated with diminished human NAFLD severity. Conversely, a pathogenic *PLIN1* frameshift variant was associated with NAFLD and fibrosis, as well as with increased hepatic RIPK3 levels in familial partial lipodystrophy.

**Conclusions:** *Ripk3* deficiency restores mitochondria bioenergetics and impacts LD dynamics. RIPK3 inhibition is promising in ameliorating NAFLD.

## INTRODUCTION

NAFLD is a complex multifactorial chronic liver disease that emerges as a result of intricate interactions of several hits, including metabolic unbalances, lipotoxicity, organelle dysfunction, and inflammation, on the top of an eventual pernicious genetic and epigenetic landscape, ultimately leading to hepatocellular injury and cell death.<sup>[1]</sup> Necroptosis is activated in the liver of human and experimental NAFLD, but the therapeutic relevance of targeting necroptosis is unclear.<sup>[2–8]</sup> Necroptosis is an immunogenic-regulated cell-death modality that critically relies on mixed lineage kinase domain-like protein (MLKL) and receptor-interacting protein kinase 3 (RIPK3) activity.<sup>[2]</sup> Considering that necroptosis ultimately results in regulated cell membrane permeabilization, it is tempting to hypothesize that lipids could be involved in the regulation and execution of necroptotic signaling pathway. We recently showed that *Ripk3*-deficient mice with NASH displayed decreased hepatic infiltration of inflammatory cells, fibrosis, and preneoplastic nodules, impacting on the hepatic lipidome, likely through upregulation of peroxisome proliferator-activated receptor  $\gamma$  (PPAR $\gamma$ ).<sup>[9]</sup> Particularly, *Ripk3* deficiency increased lipogenesis and hepatic lipid accumulation to buffer excessive detrimental lipid species but reduced very long-chain fatty acids that are functionally implicated in plasma membrane disruption during necroptosis.<sup>[9–11]</sup>

PPAR $\gamma$ , a ligand-activated transcription factor, plays a broad range of biological functions, including the control of energy metabolism as well as mitochondrial biogenesis and function. Indeed, proliferator-activated receptor gamma coactivator 1 alpha (PGC1 $\alpha$ ), a master

regulator of mitochondria turnover and bioenergetics, coactivates PPAR $\gamma$ , which in turn upregulates PGC1 $\alpha$  in an autoregulatory circuit.<sup>[12,13]</sup> Thus, the protective role of *Ripk3* deletion in NASH<sup>[9]</sup> may also rely on an improved metabolic balance related to the maintenance of mitochondrial function. Accordingly, we have shown that the improvement of high-fat diet-induced experimental NASH achieved by pharmacological inhibition of RIPK1 is MLKL-dependent and, at least in part, comprises a boost in mitochondrial respiration.<sup>[5]</sup> Still, the association between necroptosis signaling and mitochondria has been controversial. In particular, RIPK3 increases aerobic respiration upon necroptotic stimuli, leading to increased generation of mitochondrial reactive oxygen species (ROS),<sup>[14,15]</sup> which in turn could activate RIPK1 autophosphorylation in a feed-forward feedback loop that ensures effective and sustained induction of necroptosis.<sup>[16]</sup> However, the role of ROS in necroptosis execution might be cell- and context-dependent,<sup>[17]</sup> and mitochondrial depletion via mitophagy does not halt necroptotic cell death.<sup>[18]</sup> Although most of these studies used relevant in vitro systems, the pathophysiological role of RIPK3 in vivo, which integrates bioenergetics, lipid metabolism, oxidative stress, and cell death, remains unknown. Here, we aimed to evaluate the role of RIPK3 in the interaction between mitochondria and lipid metabolism in NAFLD.

## MATERIALS AND METHODS

Detailed materials and methods are included in Supporting Information.

## Patient cohort

Samples of liver tissue were obtained from 22 individuals with risk factors for NAFLD and a patient with familial partial lipodystrophy (FPLD) type 4 carrying a heterozygous *PLIN1* frameshift variant,<sup>[19]</sup> who underwent diagnostic liver biopsy. All subjects gave written informed consent before taking part in this study. The procedure was approved by the Ethics Committee of the Pitié-Salpêtrière Hospital (Paris, France), and performed following the ethical guidelines of the 1975 Declaration of Helsinki.

## Animals, diets, and sample collection

Seven- to eight-week-old male C57BL/6 wild-type (WT) and *Ripk3*<sup>-/-</sup> mice were fed a choline-deficient, amino acid-defined (CDAA; Envigo) diet for 32 or 66 weeks ( $n = 6-7$  mice per experimental group)<sup>[9]</sup> with subsequent total RNA/protein extraction, quantitative real time reverse transcriptase-polymerase chain reaction, immunoblotting, and mitochondrial respiratory chain enzymatic assays. All animal experiments were carried out with the permission of the local Animal Welfare Organ in accordance with the EU Directive (2010/63/EU), Portuguese laws (DL 113/2013, 2880/2015, 260/2016, and 1/2019) for the use and care of animals in research and all relevant legislation. The experimental protocol was approved by the competent national authority, Direção Geral de Alimentação e Veterinária, Portugal. Animals received humane care in a temperature/humidity-controlled environment with 12 hours light–dark cycles, complying with the Institute's guidelines, and as outlined in the "Guide for the Care and Use of Laboratory Animals" prepared by the National Academy of Sciences and published by the National Institutes of Health (NIH publication 86-23 revised 1985). All experiments were performed by investigators accredited for directing animal experiments (FELASA level C).

## Cell culture

CRISPR/Cas9-mediated deletion of *Ripk3* was performed in AML-12 hepatocytes (LGC Standards) and in 3T3-L1 preadipocytes (LGC Standards), followed by cell culture and treatments and subsequent cellular oxygen consumption rate (OCR) measurements, viability assays, and cell staining.

## Statistical analysis

Regular statistical analysis was performed with GraphPad Prism 7 software (GraphPad Software, Inc.). The Shapiro–Wilk test was used for testing the normality of

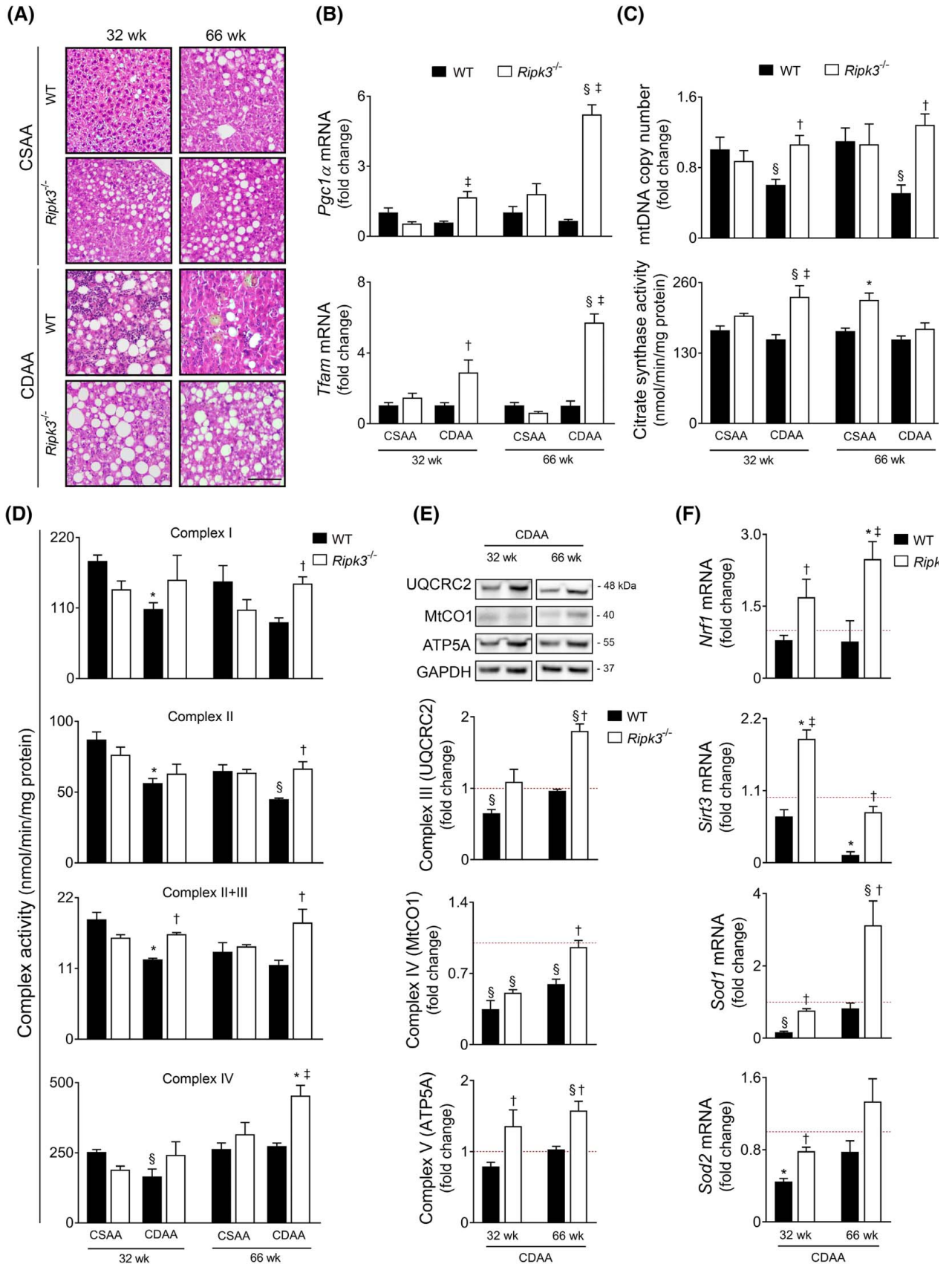
data. Student's *t* test was applied when two groups were analyzed. According to normality of values distribution, analysis of variance followed by Tukey's multiple comparison or Kruskal–Wallis followed by Dunn's multiple comparison test were performed if three or more groups were compared. Association between two variables was assessed by Pearson or Spearman correlation coefficient for normally and non-normally distributed data, respectively. Values of  $p < 0.05$  were considered statistically significant.

## RESULTS

### *Ripk3* deficiency rescues mitochondrial biogenesis and function in CDAA diet-induced experimental NASH

We have recently shown that *Ripk3* deficiency induces PPAR $\gamma$  expression in the liver of mice fed a CDAA diet or an isocaloric choline-sufficient L-amino acid-defined (CSAA) control diet for 32 and 66 weeks.<sup>[9]</sup> Because PPAR $\gamma$  is coactivated by PGC1 $\alpha$ , a master regulator of mitochondrial biogenesis and function, we investigated the role of *Ripk3* deletion in reversing mitochondrial dysfunction in experimental NASH. *Ripk3* deficiency reduced the severity of CDAA diet-induced experimental NASH (Figure 1A) while increasing hepatic mRNA and protein levels of PGC1 $\alpha$  (a significance level of at least,  $p < 0.05$ ) (Figure 1B and Figure S1A) and its target mitochondrial transcription factor A (at least,  $p < 0.05$ ) (Figure 1B and Figure S1A) after mid- and long-term CDAA feeding. CDAA diet-fed WT mice also displayed decreased mitochondrial DNA (mtDNA) copy number compared with CSAA diet-fed mice at both 32 and 66 weeks ( $p < 0.05$ ), an outcome that was abrogated by *Ripk3* deficiency ( $p < 0.05$ ) (Figure 1C), suggesting that the absence of *Ripk3* rescued impaired mitochondria biogenesis induced by the CDAA diet. Accordingly, the activity of citrate synthase, a tricarboxylic acid cycle enzyme that is also an indirect marker of mitochondrial mass, tended to increase in *Ripk3*<sup>-/-</sup> mice compared with WT mice, reaching statistical significance in mice fed the CDAA diet for 32 weeks and the CSAA diet for 66 weeks ( $p < 0.01$ ) (Figure 1C).

Then, we hypothesized that *Ripk3* deficiency mitigates the dysfunction of mitochondrial oxidative phosphorylation (OXPHOS) induced by the CDAA diet. In both WT and *Ripk3*<sup>-/-</sup> mice, CDAA diet led to decreased hepatic protein content of NADH dehydrogenase (ubiquinone) 1b subcomplex 8 at 32 and 66 weeks and succinate dehydrogenase (ubiquinone) iron–sulfur subunit at 32 weeks ( $p < 0.05$ ; Figure S1B), which are nuclear DNA-coded subunits of mitochondria respiratory chain (MRC) complexes I and II, respectively. Still, the activities of MRC complexes I and II



were restored to basal levels in *Ripk3*<sup>-/-</sup> mice at 66 weeks upon CDAA feeding ( $p < 0.05$ ) (Figure 1D). Activities of complex II + III at 32 and 66 weeks and

complex IV at 66 weeks were also rescued by *Ripk3* deficiency in CDAA diet-fed mice ( $p < 0.05$ ; Figure 1D), following the increase in mtDNA encoded ubiquinol-

**FIGURE 1** *Ripk3* deficiency rescues mitochondrial biogenesis, mitochondria respiratory chain (MRC) activity, and reactive oxygen species scavenging systems in choline-deficient, amino acid-defined (CDAA) diet-induced experimental NASH. C57BL/6 wild-type (WT) or *Ripk3*<sup>-/-</sup> mice were fed a CDAA or an isocaloric control choline-sufficient L-amino acid-defined (CSAA) diet for 32 or 66 weeks. (A) Representative images of hematoxylin and eosin-stained liver sections. Scale bar = 100  $\mu$ m. (B) qRT-PCR analysis of *Pgc1 $\alpha$*  and *Tfam* in mouse liver. (C) Quantification of relative mitochondrial DNA copy number assessed by qPCR analysis of mitochondria-encoded gene *mt-Co1*. Nuclear *Rn18s* was used as loading control (top); and citrate synthase activity determined as described in Supplementary Materials and Methods (bottom). (D) MRC activity determined as described in Supplementary Materials and Methods. (E) Immunoblotting and densitometry of oxidative phosphorylation protein complexes in mouse liver, namely UQCRC2 (CIII), mtCO1 (CIV), and ATP5A (CV). Blots were normalized to endogenous GAPDH. (F) qRT-PCR analysis of *Nrf1*, *Sod1*, *Sod2*, and *Sirt3* in mouse liver. Results are expressed as mean  $\pm$  SEM arbitrary units or fold change of 6–7 individual mice. Red dashed line represents the CSAA diet-fed WT mice levels.  $^{\$}p < 0.05$  and  $^*p < 0.01$  from CSAA diet-fed WT mice;  $^{\dagger}p < 0.05$  and  $^{\ddagger}p < 0.01$  from CDAA diet-fed WT mice.

cytochrome c reductase core protein II from complex III and cytochrome c oxidase subunit I (MTCO1) from complex IV in *Ripk3*<sup>-/-</sup> mice compared with WT ( $p < 0.05$ ) (Figure 1E). Finally, although CDAA diet did not impact ATP synthase subunit a (ATP5A) protein levels from complex V, which uses the proton-motive force created by MRC complexes I, III, and IV to generate ATP, *Ripk3* deficiency increased ATP5A protein irrespective of diet and time point (at least,  $p < 0.05$ ) (Figure 1E). Collectively, RIPK3 may contribute to impairment of OXPHOS machinery in experimental NAFLD.

PGC1 $\alpha$  also increases the expression of nuclear respiratory factors (NRFs), which are transcription factors that regulate the expression of nuclear DNA genes encoding subunits of MRC complexes and regulate oxidative stress.<sup>[13]</sup> In line with MRC complex expression and activity, liver NRF1 mRNA and protein were increased in *Ripk3*<sup>-/-</sup> mice compared with WT mice under a CDAA diet, most notably at 66 weeks (at least,  $p < 0.05$ ; Figure 1F and Figure S1C). Similarly, sirtuin 3 (SIRT3), a major mitochondria NAD<sup>+</sup>-dependent deacetylase that participates in the antioxidant defense and interacts with subunits of MRC complexes I and II, increasing their activity,<sup>[20]</sup> was upregulated in CDAA diet-fed *Ripk3*<sup>-/-</sup> mice (at least,  $p < 0.05$ ) (Figure 1F and Figure S1C), particularly at 32 weeks. The expression of superoxide dismutase 1 and 2 was also increased in the liver of CDAA diet-fed *Ripk3*<sup>-/-</sup> mice ( $p < 0.05$ ) (Figure 1F and Figure S1C). Thus, although mitochondria, particularly the MRC, play a major role in perpetuating oxidative stress under pathological conditions,<sup>[21]</sup> several enzymes that detoxify ROS are induced by *Ripk3* deficiency during CDAA feeding for 32 and 66 weeks. In agreement, we have previously shown that *Ripk3*<sup>-/-</sup> mice fed a CDAA diet for 66 weeks displayed lower hepatic levels of ROS comparing with WT mice.<sup>[9]</sup> Finally, mitofusin 2 (MFN2) promotes outer mitochondrial membrane fusion while also regulating cellular energy and mitochondrial metabolism.<sup>[22]</sup> Accordingly, MFN2 protein levels were significantly increased in CDAA diet-fed *Ripk3*<sup>-/-</sup> mice, compared with WT counterparts ( $p < 0.05$ ) (Figure S1D). Conversely, mitochondrial fission is controlled mainly by the dynamin-related protein-1, which was

upregulated in CDAA diet-fed WT mice at both 32 and 66 weeks ( $p < 0.05$ ), an outcome that is prevented by *Ripk3* deficiency at 32 weeks ( $p < 0.05$ ) (Figure S1D). Overall, *Ripk3* deficiency contributes to metabolic homeostasis in response to NASH-related hepatic stress, improving mitochondria biogenesis, metabolic reprogramming, and antioxidant defense mechanisms.

### ***Ripk3* deficiency impacts hepatocyte transcriptome improving mitochondrial bioenergetics**

We next asked whether the recovery of hepatic MRC subunit expression and activity observed in *Ripk3*<sup>-/-</sup> mice results from an overall improvement of NAFLD pathology and/or from specific modulation by RIPK3-dependent signaling pathways. CRISPR/Cas9-mediated deletion of *Ripk3* was conducted in the immortalized murine hepatocyte cell line AML-12 (Figure S2A), in which lipid metabolism and expression of mitochondrial complexes mimic that of primary mouse hepatocytes.<sup>[23]</sup> The nonsupervised principal component analysis of the transcriptome data of WT and *Ripk3*<sup>-/-</sup> AML-12 cells in the presence or absence of 125  $\mu$ M palmitate (PA) bound to bovine serum albumin for 24 h showed four distinct clusters according to genotype and stimulus (Figure 2A). A similar range and distribution of reads across all samples was observed confirming a comparable transcriptomic coverage. A total of 2894 differentially expressed genes (DEGs;  $\text{padj} \leq 0.05$ ,  $|\log_2\text{FoldChangel}| \geq 0$ ) were detected between unchallenged WT and *Ripk3*<sup>-/-</sup> hepatocytes, 4333 DEGs were detected between PA-loaded WT and *Ripk3*<sup>-/-</sup> hepatocytes, 2174 DEGs were detected between vehicle- and PA-treated WT hepatocytes, and 1316 DEGs were detected between vehicle- and PA-treated *Ripk3*<sup>-/-</sup> hepatocytes (Figure 2B). In addition, by comparing the transcriptomes of both control AML-12 cells, 207 and 178 genes were only expressed in *Ripk3*<sup>-/-</sup> and WT hepatocytes, respectively (Figure 2C). Similarly, 243 and 208 transcripts were elevated in PA-loaded *Ripk3*<sup>-/-</sup> and WT hepatocytes, respectively (Figure 2D). The DEGs were clustered using a hierarchical clustering algorithm (Figure 2B), and Kyoto Encyclopedia of Genes



**FIGURE 2** *Ripk3* deficiency shifts the hepatocyte transcriptome. Wild-type (WT) and *Ripk3*<sup>-/-</sup> AML-12 cells were treated with 125  $\mu$ M palmitate (PA) for 24 h. (A) Score scatter plot corresponding to a principal component analysis (PCA) of the RNA sequencing data. Each individual is represented by one dot. (B) Heatmap of RNA-Seq expression z scores computed for all genes that are differentially expressed between (padj  $\leq$  0.05,  $\log_2$ FoldChange  $\geq$  0), where red indicates overexpressed transcripts and blue represents underexpressed transcripts. (C) Venn diagrams showing genes expressed in unchallenged *Ripk3*<sup>-/-</sup> versus WT hepatocytes. Kyoto Encyclopedia of Genes and Genomes (KEGG) pathway enrichment analysis of upregulated and downregulated differentially expressed genes (DEGs). (D) Venn diagrams showing genes expressed in PA-treated *Ripk3*<sup>-/-</sup> versus WT hepatocytes. KEGG pathway enrichment analysis of upregulated and downregulated DEGs. (E) Heatmap of z scores of DEGs associated with the KEGG pathways oxidative phosphorylation relative to the comparison *Ripk3*<sup>-/-</sup> versus WT hepatocytes treated with PA. Each row in the heatmap is an individual sample. Red indicates overexpressed transcripts and blue represents underexpressed transcripts. \* $p$  < 0.05 from respective control.

enrichment analysis showed that mitochondria respiration-related proteins were overrepresented among the cellular components that were upregulated in *Ripk3*<sup>-/-</sup> hepatocytes compared with WT cells (Figure S3). Those include several subunits of cytochrome c oxidase and ATP synthase (Figure 2E), which were also increased in the liver of CDAA diet-fed *Ripk3*<sup>-/-</sup> mice (Figure 1E).

Next, we assessed the mitochondrial respiration of WT and *Ripk3*<sup>-/-</sup> AML-12 cells exposed to 62.5  $\mu$ M PA for 48 h (Figure 3A), a concentration that did not impact cell viability as shown by resazurin metabolism (Figure S2B). During mitochondrial respiration assays, ATP synthesis-linked respiration is determined by adding the ATP synthase inhibitor oligomycin, whereas remaining basal respiration not coupled to ATP generation is considered the proton leak. Maximal OCR is revealed by injecting the uncoupler p-trifluoromethoxy carbonyl cyanide phenyl hydrazone. Spare respiratory capacity representing the ability of a cell to respond to increased metabolic demands is calculated as the difference between maximal and basal respiration. Finally, the injection of rotenone and antimycin, inhibitors of MRC complexes I and III, respectively, allow for the determination of nonmitochondrial OCR. Our results showed that the presence of PA resulted in an approximately 30%–40% reduction of basal ( $p$  < 0.01), ATP-linked ( $p$  < 0.01), maximal ( $p$  < 0.05), and spare ( $p$  < 0.05) OCR only in WT AML-12 cells, whereas *Ripk3*<sup>-/-</sup> hepatocytes maintained mitochondrial bioenergetics after PA exposure (Figure 3B). Proton leak and nonmitochondrial respiration remained unchanged in both PA-loaded WT and *Ripk3*<sup>-/-</sup> AML-12 cells (Figure 3B). Altogether, the absence of *Ripk3* impacts on hepatocyte transcriptomic profile by increasing the expression of genes implicated in mitochondria bioenergetics and function and rescuing mitochondria respiration after free fatty acid overload.

### **Ripk3** deficiency dampens mitochondrial dysfunction and oxidative stress

Free fatty acids can modulate mitochondria ROS generation by uncoupling or by interference with MRC.<sup>[24]</sup> Mitochondrial ROS were increased in WT

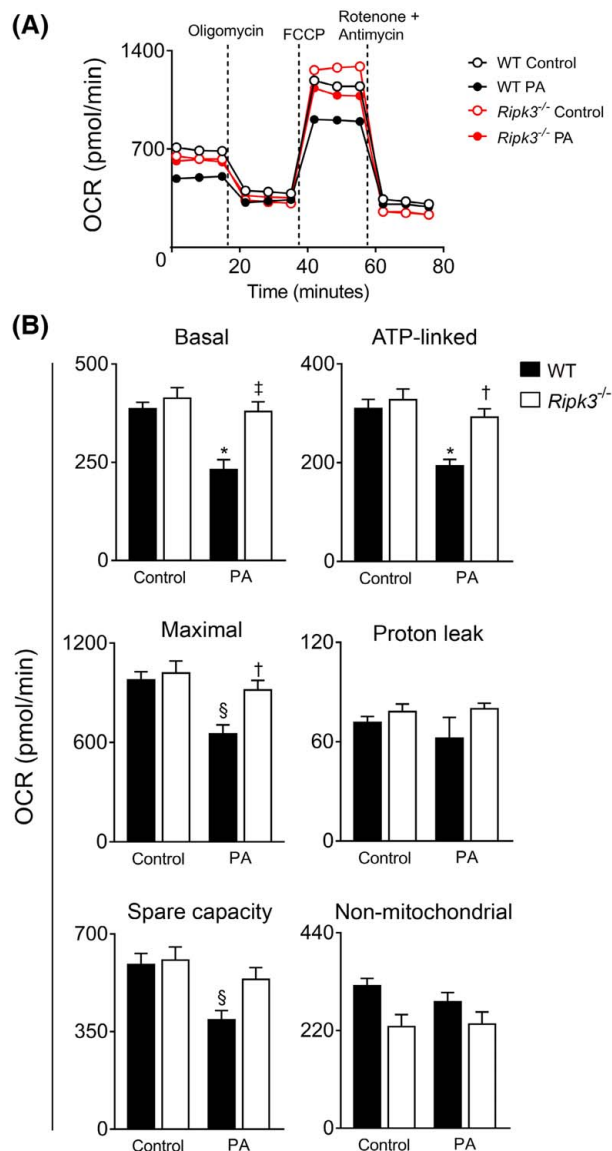


**FIGURE 3** *Ripk3* deficiency improves hepatocyte mitochondrial bioenergetics following palmitate (PA) treatment in AML-12 cells. Wild-type (WT) and *Ripk3*<sup>-/-</sup> AML-12 cells were treated with 62.5  $\mu$ M PA for 48 h. (A) Respiratory flux profiles of cells were determined using a Seahorse extracellular flux analyzer as described in Supplementary Materials and Methods. (B) Quantification of bioenergetic parameters including oxygen consumption rate (OCR) associated with basal respiration, ATP-linked, maximal respiration capacity, proton leak, spare capacity, and nonmitochondrial respiration. Results are expressed as mean  $\pm$  SEM arbitrary units of four independent experiments. § $p$  < 0.05 and \* $p$  < 0.01 from control; † $p$  < 0.05 from and ‡ $p$  < 0.01 from respective control.

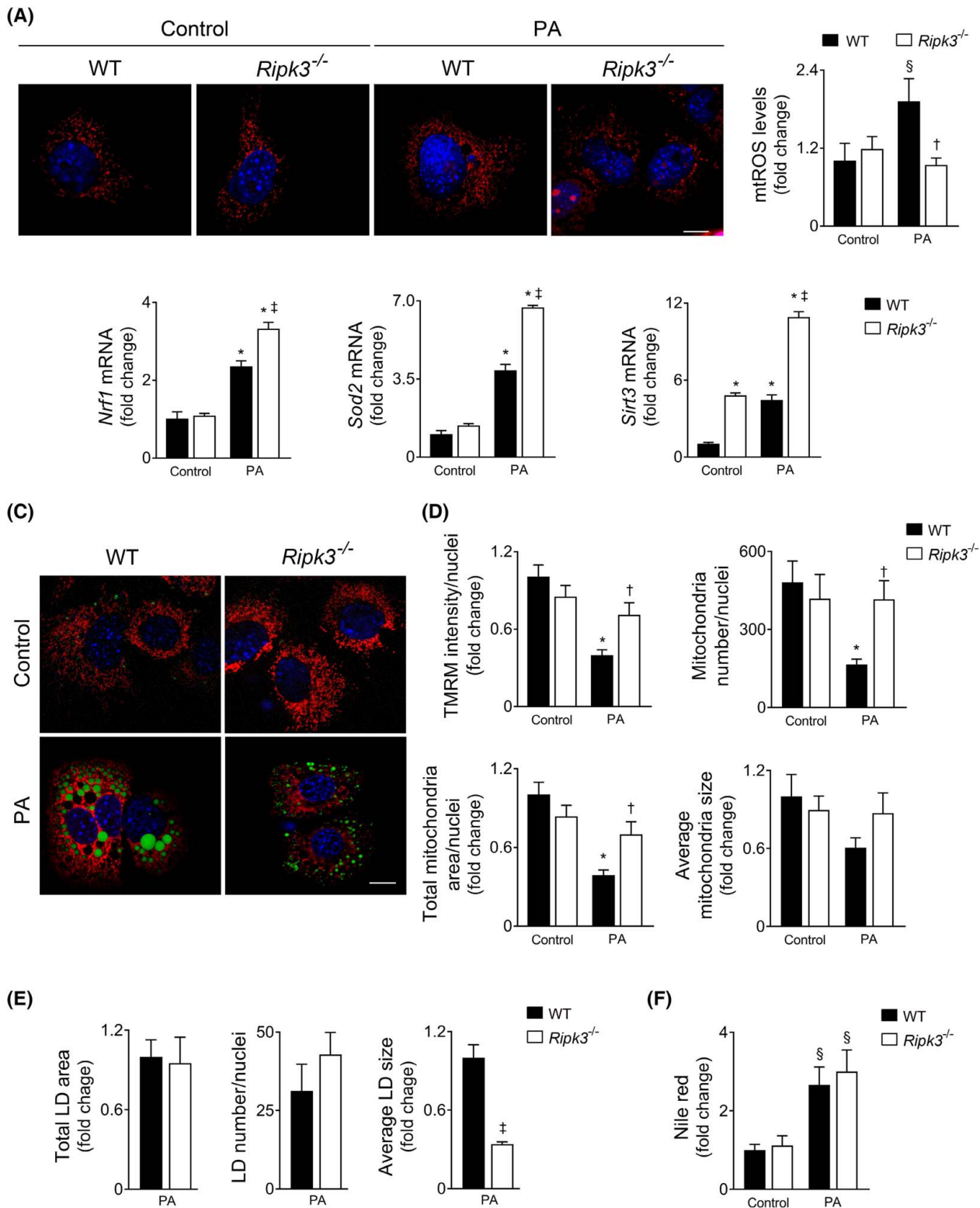


**FIGURE 4** *Ripk3* deficiency dampens hepatocyte mitochondrial reactive oxygen species (ROS) following palmitate treatment in AML-12 cells. Wild-type (WT) and *Ripk3*<sup>-/-</sup> AML-12 cells were treated with 125  $\mu$ M palmitate (PA) for 24 h. (A) Representative staining for MitoSOX Red (red). Nuclei were counterstained with Hoechst 33258 (blue). Scale bar = 85  $\mu$ M. Histogram shows the quantification of mitochondrial ROS. (B) qRT-PCR analysis of *Nrf1*, *Sod2*, and *Sirt3* in AML-12 cells. (C) Representative staining for tetramethylrhodamine methyl ester perchlorate (TMRM) (red), LipidTOX Green (green), and Hoechst 33342 (blue) for mitochondrial network, neutral LD, mitochondrial superoxide, and nuclei, respectively. Scale bar = 85  $\mu$ M. (D) Histograms show the quantification of TMRM intensity and number, area, and average size of mitochondria. (E) Histograms show the quantification of total area, average size, and number of lipid droplets. (F) Fluorometric measurement of Nile red staining normalized by SRB method. Results are expressed as mean  $\pm$  SEM fold change or percentage of four independent cultures from each genotype  $^{\S}p < 0.05$  and  $^*p < 0.01$  from control;  $^{\ddagger}p < 0.05$  from and  $^{\ddagger}p < 0.01$  from respective control.



AML-12 cells treated with 125  $\mu$ M PA for 24 h ( $p < 0.05$ ) (Figure 4A), whereas transcripts for *Nrf1* ( $p < 0.01$ ), *Sod2* ( $p < 0.01$ ), and *Sirt3* ( $p < 0.01$ ) (Figure 4B) were also increased as an adaptative cellular mechanism. In turn, *Ripk3*<sup>-/-</sup> AML-12 cells were protected from mitochondrial ROS induced by PA ( $p < 0.05$ ; Figure 4A), at least in part, by a more robust upregulation of radical scavenger systems ( $p < 0.01$ ) (Figure 4B). We also evaluated mitochondrial network morphology and mitochondrial membrane potential using the fluorescent probe tetramethylrhodamine methyl ester perchlorate (TMRM). A decrease in TMRM fluorescence intensity was observed in PA-loaded WT cells ( $p < 0.01$ ), indicating decreased mitochondrial membrane polarization, which was restored by *Ripk3* deficiency ( $p < 0.05$ ) (Figure 4C,D). TMRM labelling also showed that PA treatment reduced the number and area of polarized mitochondria only in WT AML-12 cells ( $p < 0.05$ ) (Figure 4C,D), whereas the maintenance of the mitochondrial network in PA-treated *Ripk3*<sup>-/-</sup> cells ( $p < 0.05$ ) (Figure 4D) was accompanied by a robust increase in *Pgc1 $\alpha$*  mRNA levels ( $p < 0.01$ ) (Figure S4A) downstream to PPAR $\gamma$  activation (at least  $p < 0.05$ ) (Figure S5). In addition, although the average size of mitochondria was not significantly impacted by the presence of PA and RIPK3 (Figure 4D), transcripts for optic atrophy protein (*Opa1*) and *Mfn2*, mitochondrial fusion-related genes, were increased in PA-treated *Ripk3*<sup>-/-</sup> cells (at least  $p < 0.05$ ) (Figure S4A). Collectively, *Ripk3* deficiency dampens mitochondrial dysfunction induced by PA in hepatocytes.

### **Ripk3 deficiency upregulates lipid droplet coat proteins in hepatocytes in experimental NAFLD and in patients**

Channeling PA into triglyceride droplet formation has a protective effect by preventing the generation of lipotoxic intermediates.<sup>[25]</sup> Indeed, while reducing lipidosis, inhibition of triglyceride synthesis exacerbates liver damage and fibrosis in obese mice with NASH.<sup>[26]</sup> We have shown that *Ripk3*<sup>-/-</sup> hepatocytes display increased hepatic lipid content under both hypercaloric CSAA and CDAA diets, as well as after PA exposure in vitro.<sup>[9]</sup> In agreement, here we showed that the 125- $\mu$ M PA-induced intracellular fat accumulation, as measured by Nile red fluorometric quantification, was higher in *Ripk3*<sup>-/-</sup> cells than in WT AML-12 cells at 48 h (Figure S2C). However, although the total area of lipid droplets (LDs) (Figure 4C,E) and intracellular neutral fat accumulation (Figure 4F) were similar between PA-loaded WT and *Ripk3*<sup>-/-</sup> AML-12 cells at 24 h, a higher number of smaller ( $p < 0.01$ ) LDs were found in *Ripk3*<sup>-/-</sup> cells (Figure 4C,E). Rescue experiments revealed that prior to necroptotic-associated cell swelling, overexpression of GFP-tagged murine RIPK3

enlarged LDs after free fatty acid exposure when compared with neighboring *Ripk3*<sup>-/-</sup> AML-12 cells ( $p < 0.05$ ) (Figure S4B), cosubstantiating the role of RIPK3 on LD dynamics. The impact of *Ripk3* deficiency on LD structure was independent of the modulation of lipophagy at this time point, as the decreased microtubule-associated protein LC3-II levels and increased p62 levels indicated a decrease in autophagy in PA-exposed hepatocytes regardless of genotype (Figure S4C).

LDs are not stable lipid depots, and their size and protein composition are cell context-dependent. The perilipins (PLINs) are a major family of five LD-associated proteins that regulate lipid storage and hydrolysis. Here, we evaluated the expression of the most well-known PLINs (*Plin1*, *Plin2*, and *Plin5*) in AML-12 cells and in the CDAA model. Our results showed that basal mRNA levels of *Plin1* and *Plin5* were already significantly increased in *Ripk3*<sup>-/-</sup> AML-12 cells compared with WT cells (at least  $p < 0.05$ ) and further increased with PA treatment at 24 h ( $p < 0.01$ ) (Figure 5A). In turn, *Plin2* mRNA levels were increased by PA in a dose-dependent manner in both WT and *Ripk3*<sup>-/-</sup> cells, although *Plin2* upregulation was more pronounced in *Ripk3*<sup>-/-</sup> AML-12 cells treated with the highest dose of PA (at least  $p < 0.05$ ) (Figure 5A). The transcription of *Plin1* and *Plin5* was also markedly increased in *Ripk3*<sup>-/-</sup> mice fed a CDAA diet compared with WT mice ( $p < 0.05$ ), whereas *Plin2* mRNA levels were only modestly affected by *Ripk3* deficiency (Figure 5B). PLIN1 and PLIN5 protein levels were also increased in CDAA diet-fed *Ripk3*<sup>-/-</sup> mice at both 32 and 66 weeks of feeding ( $p < 0.05$ ) and even slightly augmented in CSAA diet-fed *Ripk3*<sup>-/-</sup> mice compared with WT mice (Figure 5C). Similarly, in the adipose tissue, in which PLIN1 is highly expressed, *Plin1* mRNA levels were increased in *Ripk3*<sup>-/-</sup> mice fed either CSAA or CDAA diet at both time points when compared with WT mice (Figure 5D). *Plin1* transcript levels also increased in CRISPR-Cas9 *Ripk3*-null 3T3-L1 cells differentiated in adipocytes (Figure S6) compared with WT cells ( $p < 0.05$ ; Figure 5E), whereas the cell death associated with the differentiation process was reduced ( $p < 0.01$ ; Figure 5F).

A negative correlation between protein levels of PLIN1 or PLIN5 and RIPK3 was found in the liver of patients from an NAFLD cohort ( $p < 0.01$ ) (Figure 6A). PLIN5 levels were not differentially modulated by the NAFLD stage but were inversely correlated with circulating levels of liver injury (aspartate aminotransferase,  $p < 0.01$ ; alkaline phosphatase,  $p = 0.07$ ;  $\gamma$ -glutamyl transferase,  $p = 0.07$ ) (Figure S7A) and slightly decreased in higher fibrosis scores ( $p = 0.07$ ) (Figure 6B). In turn, although PLIN1 levels were increased in patients with NAFLD with more hepatic large or medium-sized LDs (steatosis score 3 vs. 2;  $p < 0.05$ ) (Figure 6C), patients with NAFLD with

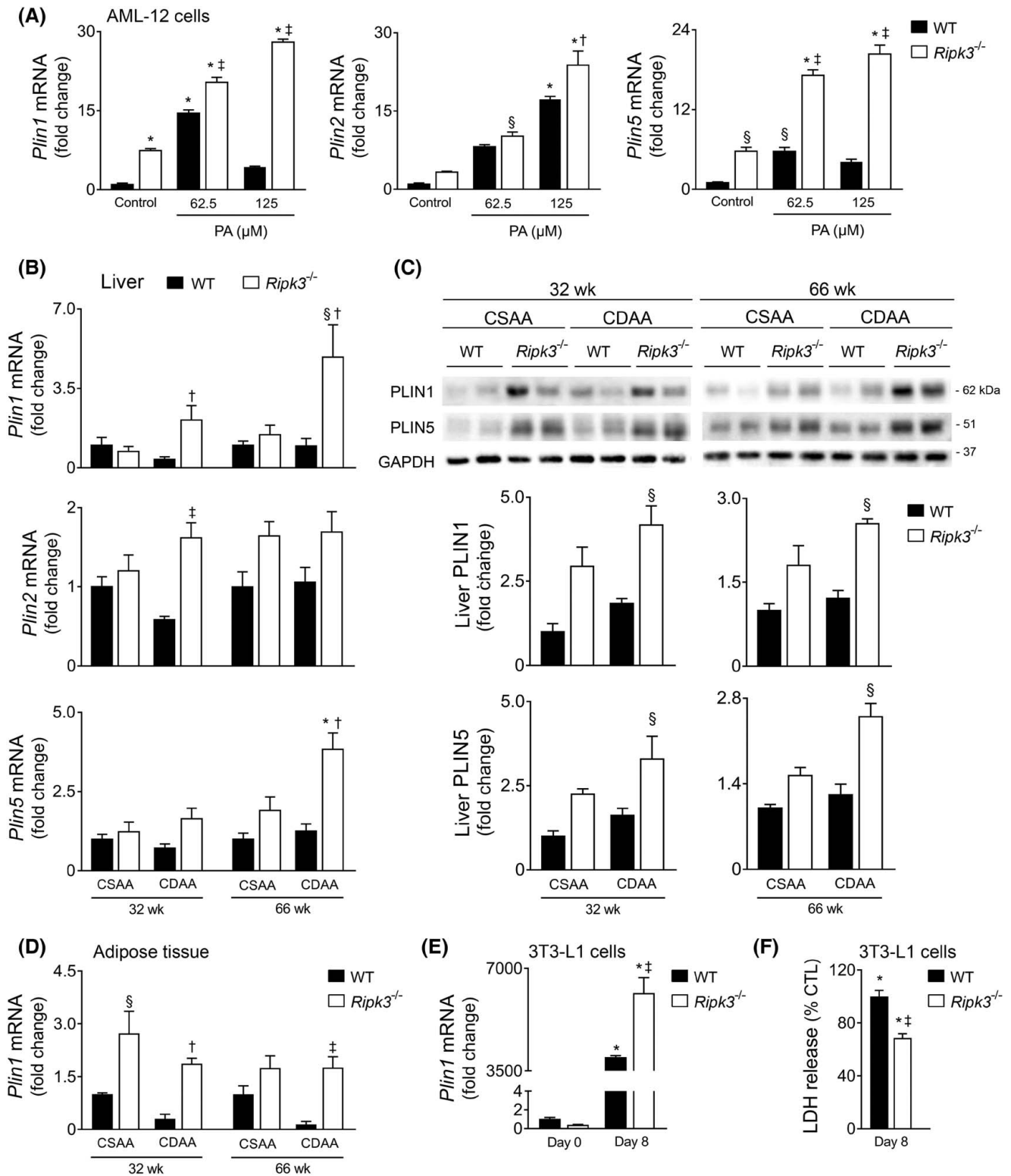


**FIGURE 5** *Ripk3* deficiency upregulates lipid droplet coat proteins in hepatocytes in vitro and in vivo. (A) qRT-PCR analysis of *Plin1*, *Plin2*, *Plin5* in wild-type (WT) and *Ripk3*<sup>-/-</sup> AML-12 cells treated with 62.5 or 125 μM palmitate for 24 h. (B) qRT-PCR analysis of *Plin1*, *Plin2*, *Plin5* in the liver of C57BL/6 WT or *Ripk3*<sup>-/-</sup> mice fed a choline-deficient, amino acid-defined (CDAA) or an isocaloric control choline-sufficient L-amino acid-defined (CSAA) diet for 32 or 66 weeks. (C) Immunoblotting and densitometry of PLIN1 and PLIN5 in the liver of C57BL/6 WT or *Ripk3*<sup>-/-</sup> mice fed a CDAA or CSAA diet for 32 or 66 weeks. Blots were normalized to endogenous GAPDH. Representative immunoblots are shown. (D) qRT-PCR analysis of *Plin1* in the white adipose tissue of C57BL/6 WT or *Ripk3*<sup>-/-</sup> mice fed a CDAA or an isocaloric control CSAA diet for 32 or 66 weeks. (E) qRT-PCR analysis of *Plin1* in WT and *Ripk3*<sup>-/-</sup> 3T3-L1 cells before (day 0) and after differentiation in adipocytes (day 8). (F) Percentage of released LDH in differentiated adipocytes relative to undifferentiated 3T3-L1 cells, as surrogate of general cells death. Results are expressed as mean ± SEM fold change or percentage to control of three to four independent in vitro experiments or six to seven individual mice. §*p* < 0.05 and \**p* < 0.01 from CSAA diet-fed WT mice; †*p* < 0.05 and ‡*p* < 0.01 from CDAA diet-fed WT mice.

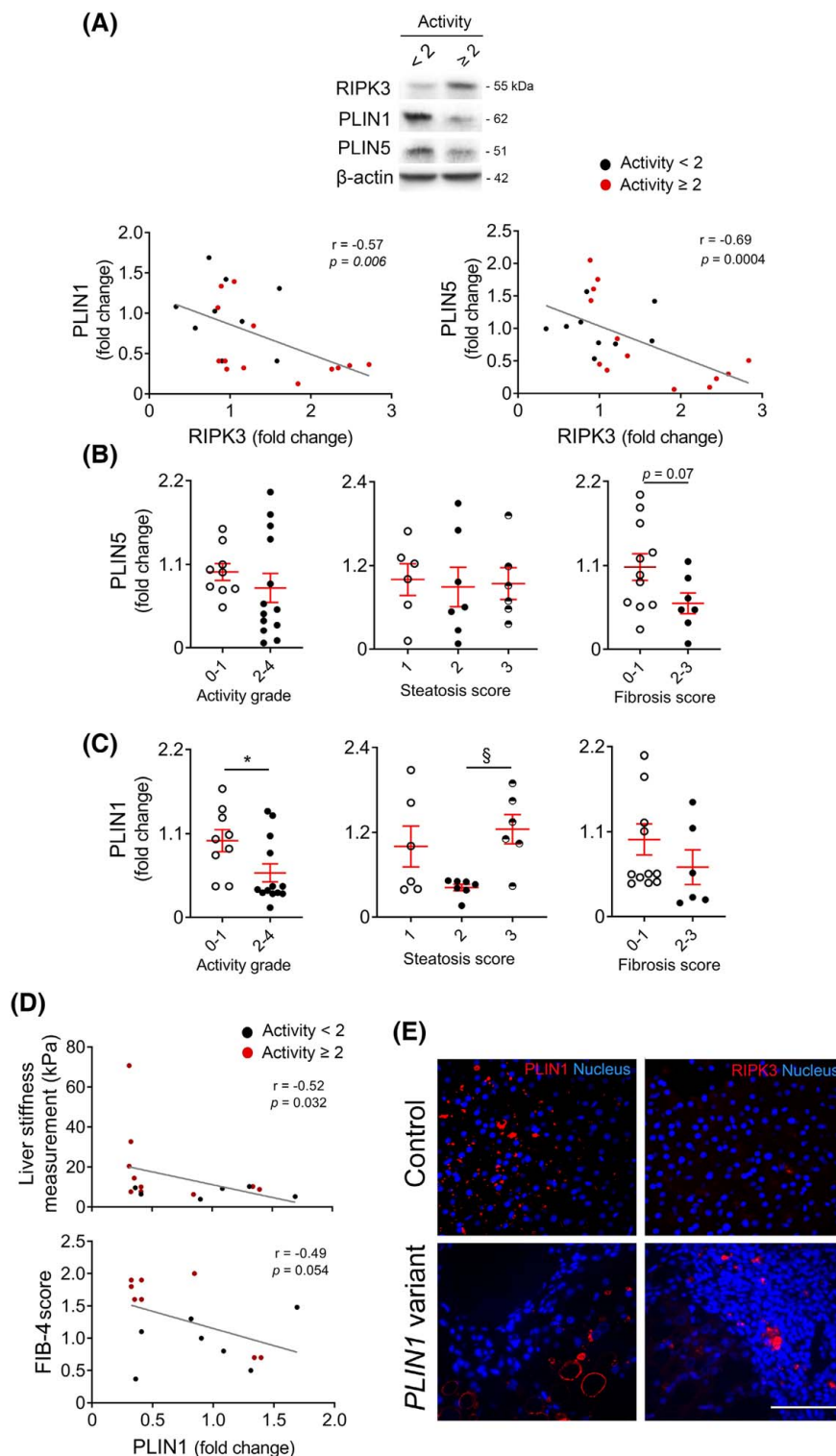


**FIGURE 6** *Ripk3* deficiency associates with augmented hepatic perilipin (PLIN)1 and PLIN5 in patients with NAFLD. (A) Representative immunoblots of RIPK3 and PLIN1 and PLIN5 in the liver of patients from an NAFLD cohort ( $n = 22$ ) and their Spearman correlation scatter plot. Blots were normalized to endogenous  $\beta$ -actin. Densitometry of PLIN1 (B) and PLIN5 (C) according to activity grade, steatosis score, and fibrosis score. Activity score in patients with NAFLD corresponds to the unweighted addition of hepatocyte ballooning and lobular inflammation as described in Supplementary Materials and Methods. (D) Spearman correlation scatter plot of hepatic PLIN1 with liver stiffness measurement assessed by FibroScan and Fibrosis-4 (FIB4) score in patients with NAFLD. Each individual is represented by one dot. Data are expressed as mean  $\pm$  SEM arbitrary units or fold change. § $p < 0.05$  and \* $p < 0.01$  compared with respective controls. (E) Representative immunostaining of PLIN1 (left) and RIPK3 (right) in liver tissue from a healthy control (top) and a patient with familial partial lipodystrophy type 4 carrying a *PLIN1* frameshift variant (bottom). Nuclei were counterstained with Hoechst 33258 (blue). Scale bar = 100  $\mu$ m.

active disease (histological activity score  $\geq 2$  vs.  $<2$ ) display diminished protein levels of PLIN1 ( $p < 0.05$ ; Figure 6C) and alkaline phosphatase ( $p < 0.05$ ) (Figure S7B). Furthermore, despite the lack of effect on fibrosis score, hepatic PLIN1 levels were negatively correlated with liver stiffness measurement ( $p < 0.05$ ) and Fibrosis-4 index ( $p = 0.054$ ) (Figure 6D). Hepatic PLIN1 levels were also decreased in diabetic and hypertensive patients with NAFLD ( $p < 0.01$ ) and with increased circulating hemoglobin A1C ( $p < 0.06$ ) (Figure S7B, C). Strikingly, a patient with FPLD type 4 carrying a 4-bp duplication in exon 8 (c.1202\_1205dup), leading to the synthesis of a p. (Pro403Argfs\*164) mutant PLIN1 protein with an altered interaction domain with 1-acylglycerol-3-phosphate O-acyltransferase (ABHD5),<sup>[19]</sup> presented severe NAFLD and liver fibrosis diagnosed at early adulthood (Table S1), without splenomegaly or biliary defect. In the liver of a patient with *PLIN1*-associated FPLD, only part of the LDs colocalized with PLIN1 (Figure S8), whereas RIPK3 protein levels increased in injured liver tissue (Figure 6E), suggesting a bidirectional functional link between PLIN1 and RIPK3 in NAFLD severity. Taken together, *Ripk3* deficiency strongly associates with upregulation of liver *Plin1* and *Plin5* in experimental NAFLD and in human NAFLD, likely playing a role in LD dynamics and disease pathogenesis.

### PLIN1 upregulation in *Ripk3*-deficient hepatocytes controls LD structure and diminishes mitochondrial stress upon free fatty acid overload

To evaluate the functional role of PLIN1 in fatty acid-loaded hepatocytes, AML-12 cells were transfected with an siRNA-targeting *Plin1*, leading to an approximately 60%–75% decrease in *Plin1* mRNA levels, compared with siRNA-control transfected cells ( $p < 0.05$ ) (Figure 7A). The absence of *Ripk3* protected AML-12 cells from 125- $\mu$ M PA-induced cell membrane permeabilization (Figure 7B), whereas the cosilencing of *Plin1* had no impact on cell viability or on neutral lipid storage in hepatocytes at 24 h (Figure 7B,C). Still, *Plin1* resulted in fewer ( $p < 0.01$ ) and enlarged LD in *Ripk3*<sup>-/-</sup> AML-12 cells at 24 h ( $p < 0.05$ ) (Figure 7D), corroborating that the upregulation of *Plin1* observed in PA-loaded *Ripk3*<sup>-/-</sup> hepatocytes shape LD morphology at early time points.

PLIN1 interacts with MFN2 in the outer mitochondrial membrane, which is key for transferring fatty acids to mitochondria in brown adipose tissue.<sup>[22]</sup> Here, we found that the knockdown of *Plin1* diminished *Mfn2* mRNA levels only in *Ripk3*<sup>-/-</sup> AML-12 cells after PA exposure ( $p < 0.01$ ), which was accompanied by a slight decrease in the mRNA levels of carnitine palmitoyltransferase I ( $p = 0.07$ ) (Figure 7E). Curiously, *Plin1* downregulation in

PA-loaded *Ripk3*<sup>-/-</sup> AML-12 cells also restored *Sod2* mRNA levels to those of PA-loaded WT cells (Figure 7E), abolishing protection against PA-induced mitochondrial ROS generation that was achieved by *Ripk3* deficiency ( $p < 0.05$ ) (Figure 7F). The contacts between mitochondria and LD have also been functionally implicated in triacylglycerol synthesis and LD expansion,<sup>[27]</sup> whereas adipose-specific *Mfn2* knockout mice display reduced transcription of acetyl-CoA carboxylase (*Acc*) and *PPAR* $\gamma$ , implicated in lipogenesis.<sup>[22]</sup> Similarly, upon PA exposure, the siRNA-mediated silencing of *Plin1* abrogated the *Ripk3*<sup>-/-</sup>-dependent upregulation of *Acc* ( $p < 0.01$ ) and *Ppar* $\gamma$  ( $p < 0.01$ ) (Figure 7E). In murine adipocytes, the expression of the *Plin1* gene is regulated by *PPAR* $\gamma$ <sup>[28]</sup>; however, although *Ppar* $\gamma$  knockdown decreased the basal expression of *Plin1* in both WT and *Ripk3*<sup>-/-</sup> AML-12 cells ( $p < 0.01$ ), the upregulation of *Plin1* in response to PA exposure was not affected by *Ppar* $\gamma$  silencing (Figure S5). Overall, *Ripk3* deficiency in hepatocytes led to an upregulation of *Plin1* that modulates LD structure and metabolism, together with the protection against mitochondrial stress upon free fatty acid overload, possibly by impacting on LD-mitochondria interaction.

## DISCUSSION

Metabolic coupling between MRC activity and mitochondrial fatty acid oxidation is crucial to curb hepatic fat accumulation and restrain ROS overabundance. In turn, the decline of mitochondrial function aggravates metabolic disturbances and may potentially contribute to NAFLD progression. On the other hand, free fatty acid overload leads to impaired mitochondria function, with consequent ROS overproduction and defective MRC activity.<sup>[21]</sup> RIPK3 acts as a lipid metabolism regulator, and its deficiency attenuates liver damage, inflammation, oxidative stress fibrosis, and carcinogenesis, both in mouse models and human NAFLD.<sup>[3–5,8,9]</sup> However, the role of RIPK3 in mitochondrial bioenergetics and function remain unclear. Here, we found that *Ripk3* deficiency strongly impacts the hepatocyte transcriptome by increasing genes associated with OXPHOS and rescues mitochondrial biogenesis, bioenergetics, and function in experimental NASH and fat-loaded hepatocytes. Moreover, *Ripk3* deficiency was accompanied by a strong upregulation of the ROS scavenging systems, leading to diminished oxidative stress upon fat loading both in vivo and in vitro. Altogether, although accumulating evidence indicates that RIPK3/MLKL could increase mitochondrial respiration and oxidative stress in response to necroptotic stimuli,<sup>[14–16]</sup> the absence of RIPK3 also prevents NAFLD-related mitochondria damage and ROS, coupled with increased mitochondria content

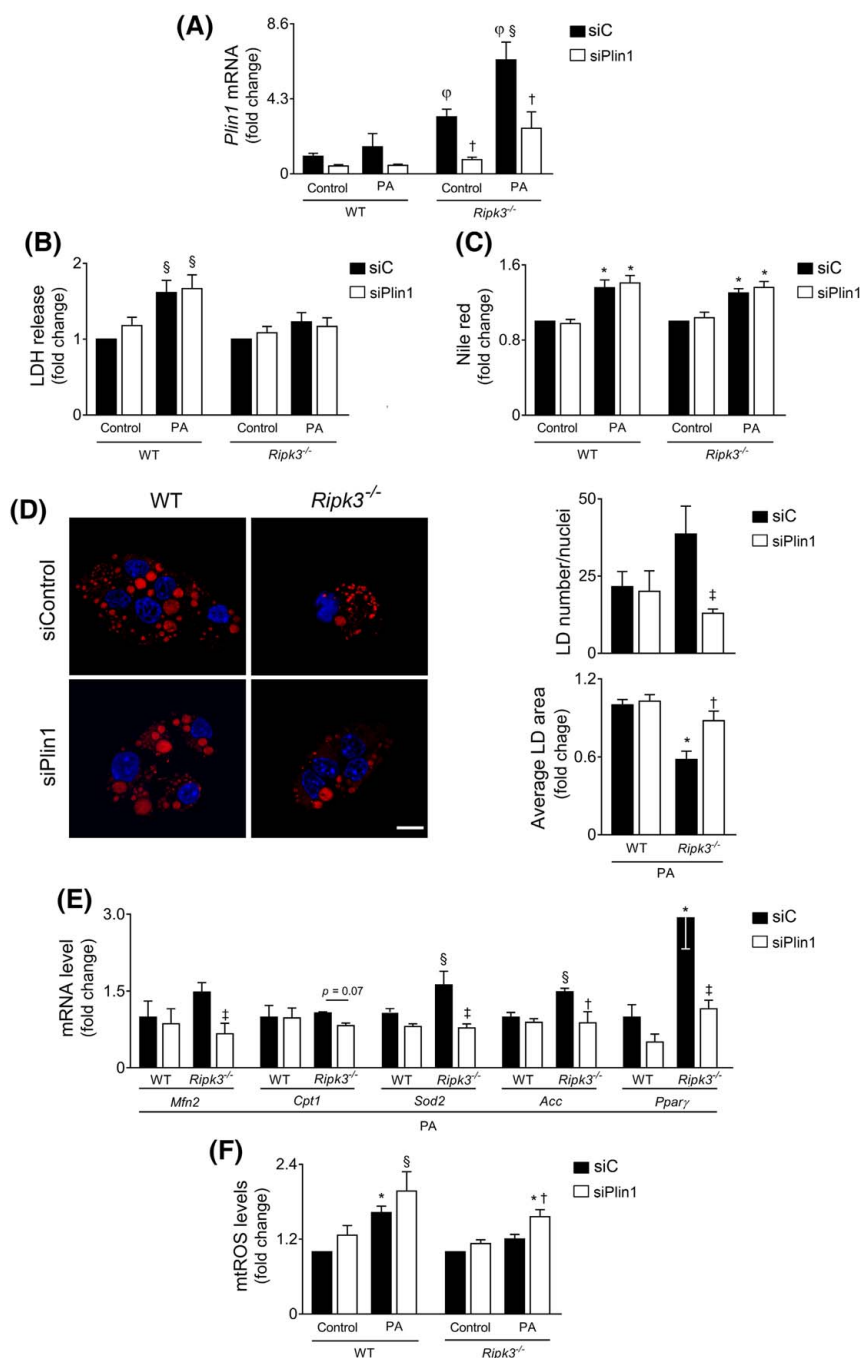


**FIGURE 7** PLIN1 upregulation in *Ripk3*-deficient hepatocytes controls lipid droplet structure and diminished mitochondrial stress upon free fatty acid overload. Wild-type (WT) and *Ripk3*<sup>-/-</sup> AML-12 hepatocytes were transfected with an siRNA-targeting *Plin1* (siPlin1) or a scrambled control (siC) for 24 h. Then, cells were loaded with 125  $\mu$ M palmitate (PA) or vehicle control for 24 h. (A) qRT-PCR analysis of *Plin1* in AML-12 cells. (B) General cell death as assessed by the lactate dehydrogenase (LDH) release assay. (C) Fluorometric measurement of Nile red staining normalized by SRB method. §*p* < 0.05 and \**p* < 0.01 from control; †*p* < 0.05 from respective control. ‡*p* < 0.05 from WT control. Data are expressed as mean  $\pm$  SEM fold change for WT control of four independent experiments. (D) Representative staining for Nile Red (red) and Hoechst 33342 (blue) for neutral lipid droplet (LD) and nuclei, respectively. Scale bar = 15  $\mu$ m. Histograms show the quantification of number and area of LD. (E) qRT-PCR analysis of *Mfn2*, *Cpt1a*, *Sod2*, *Acc*, and *Pparγ* in AML-12 cells. Data are expressed as mean  $\pm$  SEM fold change for WT PA of four independent experiments. (F) Mitochondrial reactive oxygen species as determined by the fluorometric measurement of MitoSOX Red. Data are expressed as mean  $\pm$  SEM fold change for WT control of four independent experiments. §*p* < 0.05 and \**p* < 0.01 from WT control; †*p* < 0.05 from and ‡*p* < 0.01 from respective control.

and MRC activity. The improved mitochondria fitness was likely triggered, at least in part, by increased activation of PGC1 $\alpha$ /PPAR $\gamma$  axis in *Ripk3*<sup>-/-</sup> cells, which is a pivotal pathway in lipid and metabolic

regulation, redox balance, and immune responses in NAFLD.<sup>[13,29]</sup>

LD are multifunctional and highly dynamic intracellular organelles implicated in the packaging and

management of body fat stores, critical for energy metabolism homeostasis and NAFLD development.<sup>[30]</sup> The PLIN family comprises some of the most abundant LD proteins, playing a key role in LD formation, structural remodeling, and lipolysis. PLIN1 and 2 are considered as LD *resident* proteins that are subjected to degradation when in the cytosol, whereas PLIN3, 4, and 5 are either bound to LDs or located in the cytoplasm associated with other organelles.<sup>[31]</sup> We showed that increased expression of *Plin1* in PA-loaded *Ripk3*<sup>-/-</sup> AML-12 cells was accompanied by more and smaller LDs at early time points, whereas the amount and size of LDs were recovered to WT levels upon *Plin1* loss in *Ripk3*<sup>-/-</sup> cells. Importantly, the increase in LD size can cause activation of hepatic stellate cells,<sup>[30]</sup> which we found previously decreased upon *RIPK3* knockdown.<sup>[9]</sup> Likewise, it has been shown that AML-12 cells lacking both *Plin2* and *Plin3* exhibited fewer and larger LDs, together with decreased AKT phosphorylation as a surrogate of insulin resistance.<sup>[32]</sup> This phenotype could reflect a specific function of PLINs in controlling LD life cycling and/or suggest that some PLINs present surfactant properties that minimize the contact of LD surface area with the surrounding aqueous cytosol, counteracting LD fusion. Of note, small multilocular LDs and large unilocular LDs likely show distinct profiles of interaction with their binding partners through membrane contact sites, including mitochondria. Indeed, it has been shown that the overexpression of PLIN5, which mediates the interaction between LDs and mitochondria, recruits mitochondria to LDs in multiple cell types, including AML-12 cells.<sup>[33]</sup> In adipocytes, it has been described that LD are anchored to mitochondria via a PLIN1–MFN2 interaction.<sup>[22]</sup> Here, we found that the loss-of-function of *Plin1* in *Ripk3*<sup>-/-</sup> hepatocytes led to a diminished expression of *Mfn2*, together with decreased expression of *Ppar $\gamma$*  and *Acc*, after free fatty acid exposure. Furthermore, the absence of *Ripk3* in hepatocytes treated with free fatty acids at longer time points and in livers of mice fed hypercaloric CSAA/CDAA diets<sup>[9]</sup> led to an augmented intracellular fat accumulation, accompanied by increased *Acc*, *Plin1*, and *Plin5* expression, and enhanced mitochondrial OXPHOS and citrate synthase activities. Of note, it has been reported that a higher level of mitochondria–LD contact could fuel de novo lipogenesis by increasing OXPHOS and tricarboxylic acid cycle capacity that provides ATP and citrate, respectively, which ultimately promotes the ACC-mediated production of new fatty acids<sup>[27,34]</sup>. It has also been shown that PLIN1 overexpression increases the expression of genes associated with fatty acid and triglyceride synthesis in bovine adipocytes,<sup>[35]</sup> which is also increased in the livers of *Ripk3*<sup>-/-</sup> mice from the CDAA model<sup>[9]</sup> and in PA-loaded *Ripk3*<sup>-/-</sup> AML-12 cells. Overall, these findings

suggest that PLIN1 may ultimately regulate the amount of fat produced and the interaction between LD and mitochondria in *Ripk3*<sup>-/-</sup> hepatocytes.

Increased hepatic expression of PLIN1 has been reported in patients with NAFLD.<sup>[36,37]</sup> Whether its abundance is causal or consequential to the disease is unclear. We have previously reported that *RIPK3* is increased in patients with more severe NAFLD, including those who are carriers of the rs738409 variant of the *PNPLA3* gene.<sup>[9]</sup> Here, we found that PLIN1 protein levels were negatively correlated with *RIPK3* levels in human livers and increased in patients with NAFLD with marked hepatic accumulation of large or medium-sized LDs. More importantly, PLIN1 levels were decreased in patients with more severe disease. Thus, LD growth associated with higher PLIN1 levels in hepatocytes of patients with NAFLD is likely an adaptive, beneficial, regulated phenomenon rather than a consequence of impaired utilization. Indeed, LD sustain energy and cellular homeostasis in stressed cells by controlling free fatty acid mobilization for optimal energy production and sequestering toxic lipids into their neutral lipid core.<sup>[31]</sup> Accordingly, in heterozygous *PLIN1* frameshift variant associated with FPLD<sup>[19]</sup> and severe liver fibrosis and NAFLD, only some hepatic LDs contain PLIN1, whereas *RIPK3* levels increased in injured liver tissue. Curiously, physical exercise was shown to promote an intramyocellular increase of PLIN1 and triglycerides in both control and high-fat diet–fed mice,<sup>[38]</sup> whereas the number of LDs and mitochondria and their physical interaction were also augmented in the muscle of individuals subjected to endurance exercise training.<sup>[39]</sup> Thus, we cannot exclude that upregulation of PLIN1 in other cell types could also contribute to a better phenotype in *Ripk3*<sup>-/-</sup> mice subjected to diet-induced experimental NAFLD.

Epigenetic mechanisms contribute to the regulation of *PPAR $\gamma$* , *PGC-1 $\alpha$* , and *PLIN1* during metabolic disease.<sup>[40,41]</sup> Importantly, the necroptosis-associated hepatic cytokine microenvironment is associated with lineage commitment in liver cancer by impacting on epigenome.<sup>[42]</sup> Noteworthy, we found that SIRT3, a nuclear NAD<sup>+</sup>-dependent histone deacetylase that translocates to the mitochondria upon cellular stress,<sup>[43]</sup> was augmented in *Ripk3*<sup>-/-</sup> hepatocytes both in vitro and in vivo, even at basal conditions. In line, it has been described that necroptosis is preceded by nuclear translocation of *RIPK3*<sup>[44]</sup> that directly phosphorylates and, subsequently, activates the pyruvate dehydrogenase complex,<sup>[15]</sup> which in turn converts pyruvate into acetyl-CoA. Future studies should explore whether *RIPK3* might impact the metabolic-epigenetic landscape and subsequent mitochondrial-related gene expression. In addition, *RIPK3* might also affect mitochondrial function by directly phosphorylating critical regulators of cellular metabolism, such as pyruvate dehydrogenase complex or AMP-activated protein kinase.<sup>[45]</sup>

In conclusion, the absence of RIPK3 associates with increased activation of PGC1 $\alpha$ /PPAR $\gamma$ /PLIN signaling pathways in the liver, coupled with a rescue of mitochondria content, OXPHOS machinery, and LD remodeling, as well as improved ROS detoxification capacity in experimental NAFLD. Furthermore, we uncovered a protective role of PLIN1 upregulation in the liver of patients with NAFLD. Importantly, accumulating evidence points to the role of mitochondrial maladaptation in the progression of NAFLD toward cancer. Similarly, large LDs allow rapid dynamics between lipid synthesis and consumption to sustain cell proliferation in cancer, being PLIN1 downregulated during early hepatocarcinogenesis in patients.<sup>[46]</sup> Thus, our findings may contribute to a better understanding of the mechanisms underlying the progression of NAFLD/NASH and highlight that targeting RIPK3 might provide a better metabolic adaptive response to NASH-related stress.

### AUTHOR CONTRIBUTIONS

Marta B. Afonso, Tawhidul Islam, and Julie Magusto performed most of the experiments and analyzed and interpreted results. Marta B. Afonso wrote the manuscript. Ricardo Amorim, Véronique Lenoir, Rui Simões, José Teixeira, and Liana C. Silva helped in confocal imaging and mitochondrial functional assays. Dominique Wendum, Isabelle Jéru, Corinne Vigouroux, and Vlad Ratziu provided human samples and clinical data. Rui E. Castro, Paulo J. Oliveira, Carina Prip-Buus, Vlad Ratziu, and Jérémie Gautheron provided intellectual input. Jérémie Gautheron was involved in planning and organization of the study. Cecília M. P. Rodrigues was the principal investigator of the study responsible for study concept and design. All authors critically revised the manuscript.

### ACKNOWLEDGMENTS

We thank Dr. Vishva Dixit, Molecular Oncology Department, Genentech, Inc. (San Francisco, California) and Dr. Miguel Soares, Instituto Gulbenkian de Ciência (Oeiras, Portugal) for kindly providing WT and *Ripk3*<sup>-/-</sup> from the same genetic background. We also thank Andreia Barateiro and Catarina Barros (Fernandes Lab), iMed.Ulisboa (Lisboa, Portugal) for technical support in confocal microscopy. Finally, we thank all members of Rodrigues Lab for insightful discussions.

### FUNDING INFORMATION

Main funding is provided by FEDER funds through the COMPETE programme and by national funds through Fundação para a Ciência e a Tecnologia to CMPR (grants SAICTPAC/0019/2015 – LISBOA-01-0145-FEDER-016405 and PTDC/MED-FAR/29097/2017 – LISBOA-01-0145-FEDER-029097). Additional funding comes from the European Union's Horizon 2020 Research and Innovation programme under the Marie Skłodowska-Curie Grant Agreement No. 722619 to

CMPR, CP-B and PJO. JG is funded by the Fondation pour la Recherche Médicale (ARF20170938613 & EQU202003010517), the Agence Nationale de la Recherche (ANR-21-CE18-0002-01), the Mairie de Paris (Emergences – R18139DD) and La Caixa Foundation (LCF/PR/HR21/52410028).

### CONFLICT OF INTEREST

The authors have no conflicts to report.

### DATA AVAILABILITY STATEMENT

RNAseq data are deposited on the NCBI Sequence Read Archive (SRA) under the accession number GEO Submission [GSE199155](https://www.ncbi.nlm.nih.gov/geo/query/acc.cgi?acc=GSE199155).

### ORCID

Marta B. Afonso  <https://orcid.org/0000-0003-3011-4941>

Paulo J. Oliveira  <https://orcid.org/0000-0002-5201-9948>

Vlad Ratziu  <https://orcid.org/0000-0002-6865-3791>

Cecília M. P. Rodrigues  <https://orcid.org/0000-0002-4829-754X>

### REFERENCES

1. Tilg H, Moschen AR. Evolution of inflammation in nonalcoholic fatty liver disease: the multiple parallel hits hypothesis. *Hepatology*. 2010;52:1836–46.
2. Galluzzi L, Vitale I, Aaronson SA, Abrams JM, Adam D, Agostinis P, et al. Molecular mechanisms of cell death: recommendations of the Nomenclature Committee on Cell Death 2018. *Cell Death Differ*. 2018;25:486–541.
3. Afonso MB, Rodrigues PM, Carvalho T, Caridade M, Borralho P, Cortez-Pinto H, et al. Necroptosis is a key pathogenic event in human and experimental murine models of non-alcoholic steatohepatitis. *Clin Sci (Lond)*. 2015;129:721–39.
4. Gautheron J, Vucur M, Reisinger F, Vargas Cardenas D, Roderburg C, Koppe C, et al. A positive feedback loop between RIP3 and JNK controls non-alcoholic steatohepatitis. *EMBO Mol Med*. 2014;6:1062–74.
5. Majdi A, Aoudjehane L, Ratziu V, Islam T, Afonso MB, Conti F, et al. Inhibition of receptor-interacting protein kinase 1 improves experimental non-alcoholic fatty liver disease. *J Hepatol*. 2020;72:627–35.
6. Roychowdhury S, McCullough RL, Sanz-Garcia C, Saikia P, Alkhourri N, Matloob A, et al. Receptor interacting protein 3 protects mice from high-fat diet-induced liver injury. *Hepatology*. 2016;64:1518–33.
7. Gautheron J, Vucur M, Schneider AT, Severi I, Roderburg C, Roy S, et al. The necroptosis-inducing kinase RIPK3 dampens adipose tissue inflammation and glucose intolerance. *Nat Commun*. 2016;7:11869.
8. Gautheron J, Gores GJ, Rodrigues CMP. Lytic cell death in metabolic liver disease. *J Hepatol*. 2020;73:394–408.
9. Afonso MB, Rodrigues PM, Mateus-Pinheiro M, Simao AL, Gaspar MM, Majdi A, et al. RIPK3 acts as a lipid metabolism regulator contributing to inflammation and carcinogenesis in non-alcoholic fatty liver disease. *Gut*. 2021;70:2359–72.
10. Parisi LR, Sowlati-Hashjin S, Berhane IA, Galster SL, Carter KA, Lovell JF, et al. Membrane disruption by very long chain fatty acids during necroptosis. *ACS Chem Biol*. 2019;14:2286–94.
11. Parisi LR, Li N, Atilla-Gokcumen GE. Very long chain fatty acids are functionally involved in necroptosis. *Cell Chem Biol*. 2017;24:1445–54 e1448.

12. Corona JC, Duchon MR. PPARgamma as a therapeutic target to rescue mitochondrial function in neurological disease. *Free Radic Biol Med.* 2016;100:153–63.
13. Piccinin E, Villani G, Moschetta A. Metabolic aspects in NAFLD, NASH and hepatocellular carcinoma: the role of PGC1 coactivators. *Nat Rev Gastroenterol Hepatol.* 2019;16:160–74.
14. Zhang DW, Shao J, Lin J, Zhang N, Lu BJ, Lin SC, et al. RIP3, an energy metabolism regulator that switches TNF-induced cell death from apoptosis to necrosis. *Science.* 2009;325:332–6.
15. Yang Z, Wang Y, Zhang Y, He X, Zhong CQ, Ni H, et al. RIP3 targets pyruvate dehydrogenase complex to increase aerobic respiration in TNF-induced necroptosis. *Nat Cell Biol.* 2018;20:186–97.
16. Zhang Y, Su SS, Zhao S, Yang Z, Zhong CQ, Chen X, et al. RIP1 autophosphorylation is promoted by mitochondrial ROS and is essential for RIP3 recruitment into necrosome. *Nat Commun.* 2017;8:14329.
17. Degterev A, Huang Z, Boyce M, Li Y, Jagtap P, Mizushima N, et al. Chemical inhibitor of nonapoptotic cell death with therapeutic potential for ischemic brain injury. *Nat Chem Biol.* 2005;1:112–9.
18. Tait SW, Oberst A, Quarato G, Milasta S, Haller M, Wang R, et al. Widespread mitochondrial depletion via mitophagy does not compromise necroptosis. *Cell Rep.* 2013;5:878–5.
19. Jeru I, Vantuyghem MC, Bismuth E, Cervera P, Barraud S, Group PL-S, et al. Diagnostic challenge in PLIN1-associated familial partial lipodystrophy. *J Clin Endocrinol Metab.* 2019;104:6025–32.
20. Ahn BH, Kim HS, Song S, Lee IH, Liu J, Vassilopoulos A, et al. A role for the mitochondrial deacetylase Sirt3 in regulating energy homeostasis. *Proc Natl Acad Sci U S A.* 2008;105:14447–52.
21. Mansouri A, Gattolliat CH, Asselah T. Mitochondrial dysfunction and signaling in chronic liver diseases. *Gastroenterology.* 2018;155:629–47.
22. Boutant M, Kulkarni SS, Joffraud M, Ratajczak J, Valera-Alberni M, Combe R, et al. Mfn2 is critical for brown adipose tissue thermogenic function. *EMBO J.* 2017;36:1543–58.
23. Nagarajan SR, Paul-Heng M, Krycer JR, Fazakerley DJ, Sharland AF, Hoy AJ. Lipid and glucose metabolism in hepatocyte cell lines and primary mouse hepatocytes: a comprehensive resource for in vitro studies of hepatic metabolism. *Am J Physiol Endocrinol Metab.* 2019;316:E578–89.
24. Hodson L, Gunn PJ. The regulation of hepatic fatty acid synthesis and partitioning: the effect of nutritional state. *Nat Rev Endocrinol.* 2019;15:689–700.
25. Listenberger LL, Han X, Lewis SE, Cases S, Farese RV Jr, Ory DS, et al. Triglyceride accumulation protects against fatty acid-induced lipotoxicity. *Proc Natl Acad Sci U S A.* 2003;100:3077–82.
26. Yamaguchi K, Yang L, McCall S, Huang J, Yu XX, Pandey SK, et al. Inhibiting triglyceride synthesis improves hepatic steatosis but exacerbates liver damage and fibrosis in obese mice with nonalcoholic steatohepatitis. *Hepatology.* 2007;45:1366–74.
27. Benador IY, Veliova M, Mahdavian K, Petcherski A, Wikstrom JD, Assali EA, et al. Mitochondria bound to lipid droplets have unique bioenergetics, composition, and dynamics that support lipid droplet expansion. *Cell Metab.* 2018;27:869–85 e866.
28. Dalen KT, Schoonjans K, Ulven SM, Weedon-Fekjaer MS, Bentzen TG, Koutnikova H, et al. Adipose tissue expression of the lipid droplet-associating proteins S3-12 and perilipin is controlled by peroxisome proliferator-activated receptor-gamma. *Diabetes.* 2004;53:1243–52.
29. Wang W, Xu MJ, Cai Y, Zhou Z, Cao H, Mukhopadhyay P, et al. Inflammation is independent of steatosis in a murine model of steatohepatitis. *Hepatology.* 2017;66:108–23.
30. Scorletti E, Carr RM. A new perspective on NAFLD: focusing on lipid droplets. *J Hepatol.* 2022;76:934–45.
31. Olzmann JA, Carvalho P. Dynamics and functions of lipid droplets. *Nat Rev Mol Cell Biol.* 2019;20:137–55.
32. Bell M, Wang H, Chen H, McLenithan JC, Gong DW, Yang RZ, et al. Consequences of lipid droplet coat protein downregulation in liver cells: abnormal lipid droplet metabolism and induction of insulin resistance. *Diabetes.* 2008;57:2037–45.
33. Wang H, Sreenivasan U, Hu H, Saladino A, Polster BM, Lund LM, et al. Perilipin 5, a lipid droplet-associated protein, provides physical and metabolic linkage to mitochondria. *J Lipid Res.* 2011;52:2159–68.
34. Benador IY, Veliova M, Liesa M, Shirihai OS. Mitochondria bound to lipid droplets: where mitochondrial dynamics regulate lipid storage and utilization. *Cell Metab.* 2019;29:827–35.
35. Zhang S, Liu G, Xu C, Liu L, Zhang Q, Xu Q, et al. Perilipin 1 mediates lipid metabolism homeostasis and inhibits inflammatory cytokine synthesis in bovine adipocytes. *Front Immunol.* 2018;9:467.
36. Straub BK, Stoeffel P, Heid H, Zimbelmann R, Schirmacher P. Differential pattern of lipid droplet-associated proteins and de novo perilipin expression in hepatocyte steatogenesis. *Hepatology.* 2008;47:1936–46.
37. Pawella LM, Hashani M, Eiteneuer E, Renner M, Bartenschlager R, Schirmacher P, et al. Perilipin discerns chronic from acute hepatocellular steatosis. *J Hepatol.* 2014;60:633–42.
38. Morton TL, Galior K, McGrath C, Wu X, Uzer G, Uzer GB, et al. Exercise increases and browns muscle lipid in high-fat diet-fed mice. *Front Endocrinol (Lausanne).* 2016;7:80.
39. Tarnopolsky MA, Rennie CD, Robertshaw HA, Fedak-Tarnopolsky SN, Devries MC, Hamadeh MJ. Influence of endurance exercise training and sex on intramyocellular lipid and mitochondrial ultrastructure, substrate use, and mitochondrial enzyme activity. *Am J Physiol Regul Integr Comp Physiol.* 2007;292:R1271–8.
40. Kramer AI, Handschin C. How epigenetic modifications drive the expression and mediate the action of PGC-1alpha in the regulation of metabolism. *Int J Mol Sci.* 2019;20:5449.
41. Bialesova L, Kulyte A, Petrus P, Sinha I, Laurencikiene J, Zhao C, et al. Epigenetic Regulation of PLIN 1 in obese women and its relation to lipolysis. *Sci Rep.* 2017;7:10152.
42. Seehawer M, Heinzmann F, D'Artista L, Harbig J, Roux PF, Hoenicke L, et al. Necroptosis microenvironment directs lineage commitment in liver cancer. *Nature.* 2018;562:69–75.
43. Scher MB, Vaquero A, Reinberg D. SirT3 is a nuclear NAD<sup>+</sup>-dependent histone deacetylase that translocates to the mitochondria upon cellular stress. *Genes Dev.* 2007;21:920–8.
44. Yoon S, Bogdanov K, Kovalenko A, Wallach D. Necroptosis is preceded by nuclear translocation of the signaling proteins that induce it. *Cell Death Differ.* 2016;23:253–60.
45. Wu W, Wang X, Sun Y, Berleth N, Deitersen J, Schlutermann D, et al. TNF-induced necroptosis initiates early autophagy events via RIPK3-dependent AMPK activation, but inhibits late autophagy. *Autophagy.* 2021;17:3992–4009.
46. Straub BK, Herpel E, Singer S, Zimbelmann R, Breuhahn K, Macher-Goeppinger S, et al. Lipid droplet-associated PAT-proteins show frequent and differential expression in neoplastic steatogenesis. *Mod Pathol.* 2010;23:480–92.

**How to cite this article:** Afonso MB, Islam T, Magusto J, Amorim R, Lenoir V, Simões R, et al. RIPK3 dampens mitochondrial bioenergetics and lipid droplet dynamics in metabolic liver disease. *Hepatology.* 2023;77:1319–1334. <https://doi.org/10.1002/hep.32756>